ACS OMEGA

Article

Cite This: ACS Omega 2018, 3, 12099−12105

http://pubs.acs.org/journal/acsodf

Solar-Driven One-Compartment Hydrogen Peroxide-Photofuel Cell Using Bismuth Vanadate Photoanode

Tatsuhiro Onishi,[†] Musashi Fujishima,[‡] and Hiroaki Tada*[,†,‡]

[†]Graduate School of Science and Engineering and [‡]Department of Applied Chemistry, Faculty of Science and Engineering, Kindai University, 3-4-1, Kowakae, Higashi-osaka, Osaka 577-8502, Japan

Supporting Information

ABSTRACT: One-compartment H_2O_2-photofuel cells using monoclinic scheelite $BiVO_4$ film deposited on fluorine-doped tin oxide (ms-$BiVO_4$/FTO) as the photoanode, Prussian blue film-coated FTO cathode, and deaerated aqueous electrolyte solution of 0.1 M $NaClO_4$ and 0.1 M H_2O_2 were constructed. Mesoporous TiO_2 photoanode cells with the same cathode and electrolyte solution were also prepared for comparison. The ms-$BiVO_4$/FTO photoanode was prepared by a two-step route consisting of spin coating of a precursor solution on FTO and subsequent heating at 500 °C in the air. The thickness of the ms-$BiVO_4$ film was controlled in the range from 50 to 500 nm by the number of the spin-coating times. There is an optimum thickness of the ms-$BiVO_4$ film in the cell performances under illumination of simulated sunlight (AM 1.5, 100 mW cm^{-2}, 1 sun). Under the optimum conditions, the ms-$BiVO_4$/FTO photoanode cell provides a short-circuit current (J_{sc}) = 0.81 mA cm^{-2} and an open-circuit voltage (V_{oc}) = 0.61 V, far surpassing the values of J_{sc} = 0.01 mA cm^{-2} and V_{oc} = 0.31 V for the conventional mesoporous TiO_2 photoanode cell. The striking cell performance is ascribable to the high visible-light activity of ms-$BiVO_4$ for H_2O_2 oxidation and its low thermocatalytic activity for the decomposition.

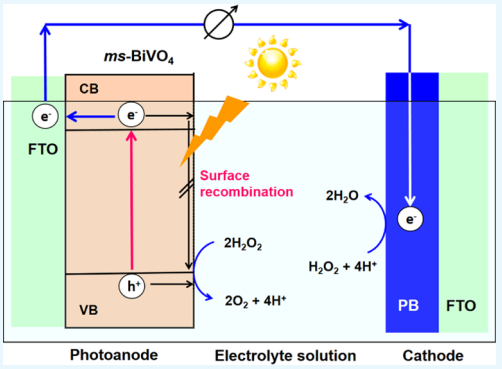

INTRODUCTION

A sustainable "solar oxygen cycle" can be completed by combining the technology for synthesizing H_2O_2 from H_2O and/or O_2 and H_2O_2-fuel cell (FC) (Scheme 1).[1] At present,

Scheme 1. Solar Oxygen Cycle with H_2O_2 as the Key Component

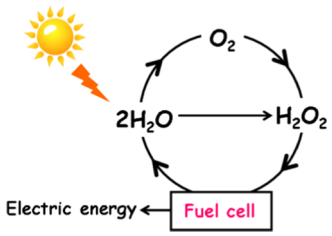

most H_2O_2 is industrially produced by the anthraquinone method with the consumption of a large amount of energy.[2] As an alternative method, photocatalytic synthesis of H_2O_2 via O_2 reduction[3−7] and H_2O oxidation[8] are currently in rapid progress. On the other hand, photofuel cells (PFCs) using TiO_2 photoanode have recently been developed as a chemical-to-electric energy conversion device.[9,10] The PFCs have attracted considerable interest because of the availability of biomass derivatives as the fuel, but the operation emits CO_2.[11,12] Meanwhile, clean one-compartment FCs can be constructed without the expensive separator by only using H_2O_2 as the fuel and oxidant.[13] We have recently reported a prototype of one-compartment H_2O_2-PFC consisting of mesoporous TiO_2 film coated on fluorine-doped tin oxide (mp-TiO_2/FTO, photoanode), glassy carbon (cathode), and an aqueous electrolyte solution of H_2O_2 (pH 3).[14] In this cell, H_2O_2 is oxidized to O_2 on the mp-TiO_2/FTO photoanode (eq 1), whereas H_2O_2 is reduced to H_2O at the cathode (eq 2).

$$H_2O_2 \rightarrow O_2 + 2H^+ + 2e^- \; E_a = +0.518 \text{ V at pH 3} \quad (1)$$

$$H_2O_2 + 2H^+ + 2e^- \rightarrow 2H_2O \; E_c = +1.586 \text{ V at pH 3} \quad (2)$$

where the electrode potentials are values with respect to the standard hydrogen electrode (SHE).

The H_2O_2-FC and H_2O_2-PFC afford a thermodynamic electromotive force (=$E_c - E_a$) of 1.07 V comparable with the value for the H_2/O_2-FC (1.23 V). In addition, the H_2O_2-PFC has various advantages over the H_2/O_2-FC, i.e., it can be easily handled at ambient temperature and pressure and does not need separator and electrocatalysts such as Pt. The most serious drawback common with these PFCs is that TiO_2 only responds to UV-light occupying a few percent of the solar spectrum.[15] The photoanode material for the H_2O_2-PFC

Received: June 13, 2018
Accepted: September 11, 2018
Published: September 27, 2018

DOI: 10.1021/acsomega.8b01333
ACS Omega 2018, 3, 12099−12105

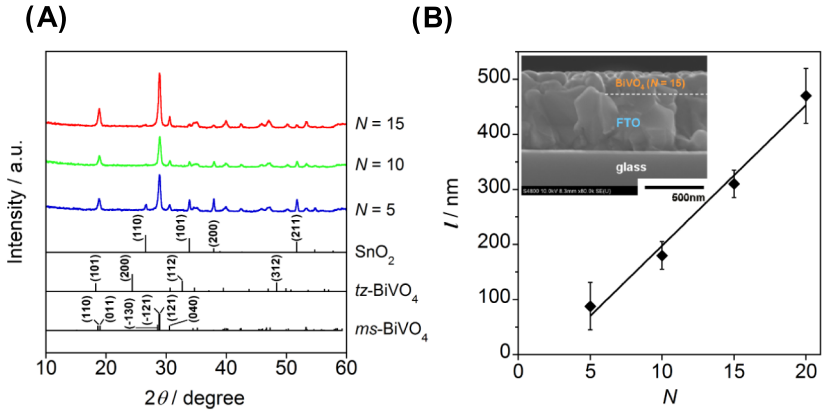

Figure 1. (A) XRD patterns of $BiVO_4$/FTO electrodes prepared at various spin-coating cycles. (B) Plots of the thickness of $BiVO_4$ film (l) vs the number of spin-coating cycle (N). The inset is the cross-sectional SEM image of the $BiVO_4$/FTO electrode.

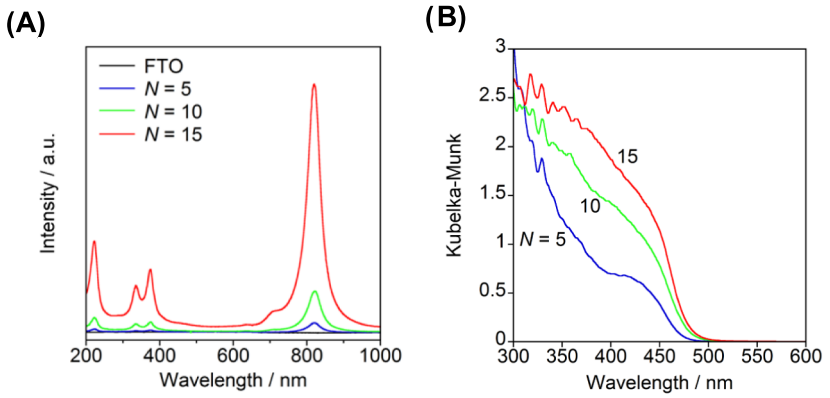

Figure 2. Raman spectra (A) and UV−vis absorption spectra (B) of $BiVO_4$/FTO electrode prepared at various spin-coating cycle. The inset shows the Tauc plots for the same samples.

should possess the following properties: (1) high visible-light activity for H_2O_2 oxidation, (2) low thermocatalytic activity for H_2O_2 decomposition, (3) high stability, and (4) nontoxicity. In the biomass-PFC, the cell performances have been improved by using a visible-light-responsive TiO_2 photoanode.[16,17] The simultaneous fulfillment of conditions (1) and (2) is a difficult subject because H_2O_2 undergoes catalytic decomposition by various materials. Among the visible-light-responsive semiconductor photocatalysts, bismuth vanadate ($BiVO_4$) is a promising material because it is known to have a high level of activity for H_2O oxidation[18] as well as high stability (condition 3) and nontoxicity (condition 4),[19] whereas Prussian blue (PB) can be used as the cathode material effectively improving the cell performances of H_2O_2-FC[20] and H_2O_2-PFC.[21] Here, we report a visible-light-driven one-compartment H_2O_2-PFC using $BiVO_4$/FTO photoanode and PB/FTO cathode and the performances under simulated sunlight.

RESULTS AND DISCUSSION

$BiVO_4$ is an n-type semiconductor with three crystal polymorphs, i.e., monoclinic scheelite (ms), tetragonal scheelite (ts), and tetragonal zircon (tz) structures. Among them, ms-$BiVO_4$ was reported to show the highest photocatalytic activity due to its narrower band gap energy (E_g) of 2.4 eV against tz-$BiVO_4$ with E_g = 2.9 eV[22] and the more significant distortion of the metal polyhedra than ts-$BiVO_4$.[23] The crystal form of the present $BiVO_4$ film was determined by X-ray diffraction (XRD) measurements. Figure 1A shows the XRD patterns for the samples prepared at various spin-coating cycles (N). In the XRD patterns, sharp diffraction peaks are present at 2θ = 18.9, 28.9, and 30.6°. The first peak is derived from the overlapping of the diffraction peaks assignable to the (110) and (011) crystal planes of ms-$BiVO_4$, the second peak to the ($\bar{1}30$), ($\bar{1}21$), and (121) planes, and the third peak to the (040) plane (ICDD 00-014-0688). Also, the diffraction peaks observed at 26.6, 33.9, 37.9, and 51.8° are assignable to the diffraction from the (110), (101), (200), and (211) crystal planes of SnO_2 (ICDD 01-070-6995), respectively. Clearly, films consisting of single-phase ms-$BiVO_4$ are formed on FTO by the spin-coating technique. As shown in the inset in Figure 1B, the scanning electron microscopy (SEM) image confirms the formation of uniform ms-$BiVO_4$ layer on the FTO surface. Figure 1B shows the relation between the thickness of ms-$BiVO_4$ (l) and N. The l increases linearly with respect to N according to the following equation of l (nm) = 25.5N − 57.0 at $N \geq 5$. In Figure 1A, the intensity of the diffraction peaks of SnO_2 monotonically decreases with an increase in N or l.

Raman spectra were recorded to gain information about the bulk and local structures of the ms-$BiVO_4$ film. Figure 2A shows the Raman spectra for ms-$BiVO_4$/FTO with varying N. Every spectrum has several signals that increase in intensity with an increase in N. In the spectrum of the sample (N = 15), the signals at 375 and 335 cm^{-1} are due to the symmetric and antisymmetric bending modes of VO_4^{3-} anion ($\delta_s(VO_4^{3-})$ and $\delta_{as}(VO_4^{3-})$), respectively. Also, the intense signal at 822 cm^{-1} and the weak signal around 710 cm^{-1} are assignable to the

DOI: 10.1021/acsomega.8b01333
ACS Omega 2018, 3, 12099−12105

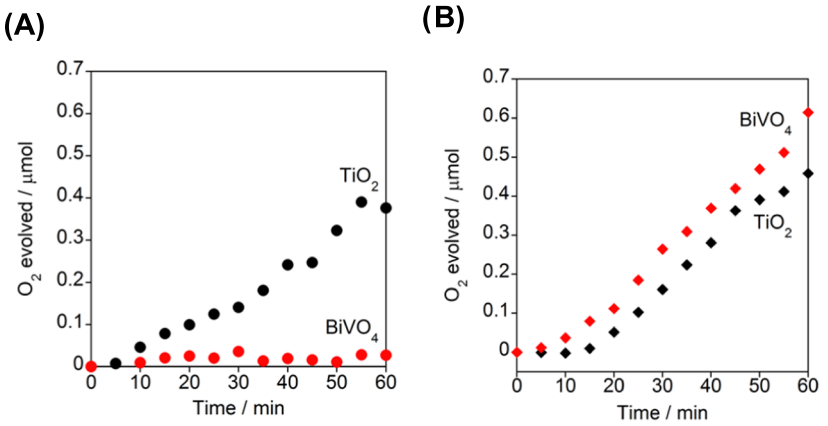

Figure 3. Time courses for O_2 evolution with the decomposition of H_2O_2 in the presence of TiO_2 particles (10 mg) or $BiVO_4$ particles (10 mg) in the dark (A) and under illumination of simulated sunlight (B, AM 1.5, 19 mW cm^{-2}).

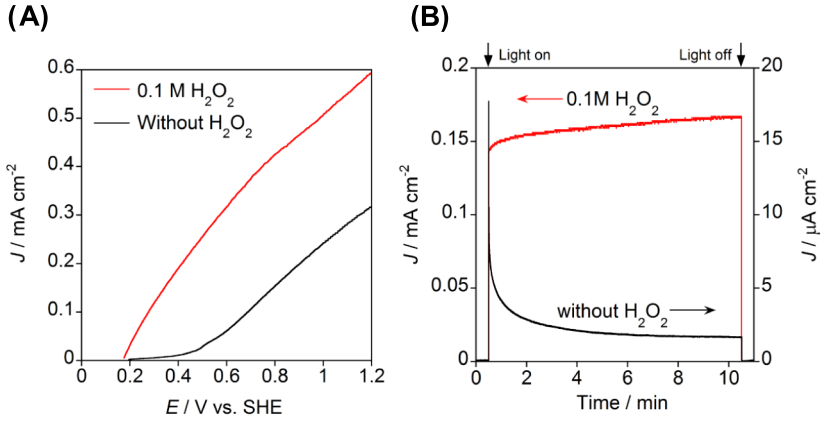

Figure 4. (A) Current (J)−electrode potential (E) curves for the three-electrode cell with the structure of $BiVO_4$/FTO photoanode (N = 5)| deaerated electrolyte solution of 0.1 M $NaClO_4$ without (black) and with (red) 0.1 M H_2O_2 (pH 3)|Ag/AgCl reference electrode|glassy carbon counter electrode under the illumination of simulated solar light (AM 1.5, 100 mW cm^{-2}, 1 sun). (B) Photochronoamperometry curves at the rest potential for the three-electrode cell with the same cell configuration as in (A).

symmetric and antisymmetric stretching vibrations of the VO_4^{3-} anion (ν_s(V−O) and ν_{as}(V−O)), respectively.[24] The emergence of the forbidden ν_{as}(V−O) band can be induced by the distortion of the local symmetry of VO_4^{3-} tetrahedron in ms-$BiVO_4$. Yu and Kudo reported that the local structure as well as crystallinity affects the photocatalytic activity of the O_2 evolution from an $AgNO_3$ aqueous solution.[25] The absence of the ν_{as}(V−O) signal in the spectrum of the sample (N = 5) is probably due to the small film thickness of ∼70 nm.[26] Figure 2B shows the UV−vis absorption spectra of ms-$BiVO_4$/FTO with varying N. Every sample has a strong absorption due to the interband transition at λ < 500 nm, whose intensity increases with increase in N. Density functional theory calculations for the ms-$BiVO_4$ crystal indicated that the valence band (VB) maximum and conduction band (CB) minimum mainly consist of the nonbonding O 2p and nonbonding V 3d states, and the interband transition is allowed along the polarization direction of $E//a$ and $E//c$.[27] The direct band gap (E_g) was determined from the $[F(R_\infty)h\nu]^2$ vs ($h\nu - E_g$) plot, where $h\nu$ is the photon energy.[28] The E_g lies in the range from 2.6 to 2.7 eV, and there is a trend that it increases with decreasing N or l. The E_g values are somewhat larger than the value of 2.45 ± 0.05 eV reported for ms-$BiVO_4$ particles at room temperature (Figure S1).[29]

The thermocatalytic and photocatalytic activities of TiO_2 and ms-$BiVO_4$ particles for H_2O_2 decomposition were examined in a deaerated 0.1 M H_2O_2 aqueous solution (pH 3). The rates of H_2O_2 decomposition in the dark and under irradiation are denoted as ν_{dark} and ν_{ph}, respectively, below. Figure 3A compares the time courses of O_2 evolution from 0.1 M H_2O_2 aqueous solution in the TiO_2 and ms-$BiVO_4$ systems in the dark. In the TiO_2 system, the amount of O_2 increases with a ν_{dark} of 0.36 μmol h^{-1}, whereas the decomposition is very sluggish in the ms-$BiVO_4$ system (ν_{dark} < 0.03 μmol h^{-1}). Clearly, ms-$BiVO_4$ is almost inert for H_2O_2 decomposition in the dark, whereas TiO_2 has a significant thermocatalytic activity.[30] Figure 3B shows time courses for O_2 evolution from 0.1 M H_2O_2 aqueous solution in the TiO_2 and ms-$BiVO_4$ systems under simulated sunlight (AM 1.5, 19 mW cm^{-2}). Irradiation of ms-$BiVO_4$ causes H_2O_2 decomposition with a ν_{ph} of 0.45 μmol h^{-1}. In the TiO_2 system, O_2 is produced with a ν_{ph} of 0.42 μmol h^{-1}. The ν_{ph}/ν_{dark} ratio for ms-$BiVO_4$ reaches 16.7, which is larger than the value for TiO_2 by a factor of 14. The high level of visible-light activity (condition 1) and low thermocatalytic activity (condition 2) of ms-$BiVO_4$ for the H_2O_2 decomposition lead us to expect its application as the photoanode material for the H_2O_2-PFC. In the absence of H_2O_2, O_2 is hardly generated in the ms-$BiVO_4$ system (Figure S2). Previously, the flatband potential of ms-$BiVO_4$ or the

DOI: 10.1021/acsomega.8b01333
ACS Omega 2018, 3, 12099−12105

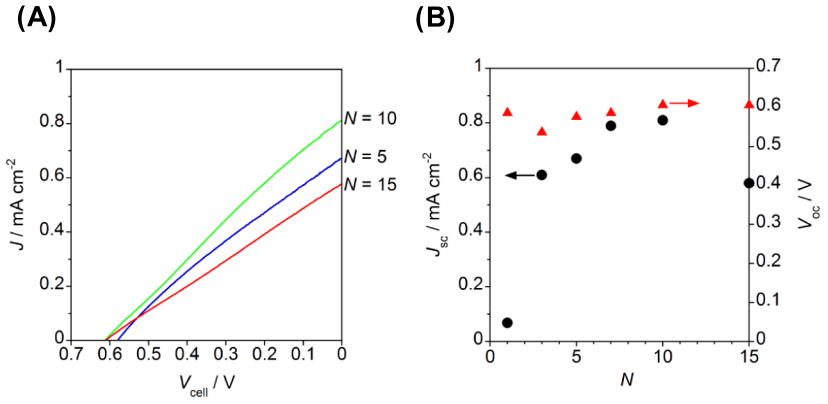

Figure 5. (A) $J-V_{cell}$ curves for the two-electrode cell with the structure of $BiVO_4$/FTO photoanode|deaerated electrolyte solution of 0.1 M $NaClO_4$ with 0.1 M H_2O_2 (pH 3)|PB/FTO cathode under the illumination of simulated solar light (AM 1.5, 100 mW cm^{-2}, 1 sun). (B) J_{sc} and V_{oc} of the H_2O_2-PFCs as functions of N.

approximate conduction band (CB) minimum potential (E_{CB}) was determined to be −0.064 V at pH 3 (SHE) by the slurry method.[31] By using this value and the E_g of 2.60 eV, the valence band (VB) maximum potential (E_{VB}) can be estimated to be +2.54 V at pH 3 (vs SHE). Thus, the potential of the excited electrons in the CB of ms-$BiVO_4$ is insufficient for H_2O reduction (electrode potential, $E(H_2O/H_2)$ = −0.177 V vs SHE at pH 3),[32] whereas the VB-holes can oxidize H_2O oxidation ($E(O_2/H_2O)$ = +1.05 V vs SHE at pH 3).[32]

To study the H_2O_2 additive effect on the photoelectrochemical (PEC) properties of ms-$BiVO_4$/FTO, three-electrode PEC cells with a structure of ms-$BiVO_4$/FTO (N = 5, working electrode)|deaerated aqueous electrolyte solution containing 0.1 M $NaClO_4$ (pH 3)|Ag/AgCl (reference electrode)|glassy carbon (counter electrode) were fabricated, and the photocurrent (J)−electrode potential (E) curves were measured for the cells under the illumination of simulated solar light (AM 1.5, 100 mW cm^{-2}, 1 sun). Figure 4A compares the $J-E$ curves of the ms-$BiVO_4$/FTO electrode in the electrolyte solutions with (red) and without 0.1 M H_2O_2 (black). In the H_2O_2-free cell, the photocurrent starts to flow around +0.4 V vs SHE. In the H_2O_2-cell, the photocurrent sharply increases at the onset potential of +0.2 V vs SHE. Figure 4B shows the photochronoamperometry curves for the PEC cells. In the H_2O_2-free cell, a sharp decay in the photocurrent is observed immediately after photoirradiation. This feature indicates that significant surface recombination occurs via surface peroxo species generated during the H_2O oxidation by the VB-holes. On the other hand, the initial anodic photocurrent spike and its subsequent decay disappear in the H_2O_2-cell, providing a very stable photocurrent. Thus, H_2O_2 works as an excellent scavenger for the VB-holes in ms-$BiVO_4$, effectively suppressing the surface recombination.[33]

The performance of one-compartment H_2O_2-PFCs were examined for the cell with a structure of ms-$BiVO_4$/FTO photoanode|deaerated aqueous electrolyte solution containing 0.1 M $NaClO_4$ and 0.1 M H_2O_2 (pH 3)|PB/FTO cathode under irradiation of simulated sunlight (AM 1.5, 100 mW cm^{-2}, 1 sun). Figure 5A exhibits the photocurrent (J)−cell voltage (V_{cell}) curves for the H_2O_2-PFCs using ms-$BiVO_4$/FTO photoanodes prepared at varying N. The $J-V_{cell}$ curves are highly dependent on N. Figure 5B shows the N-dependences of the short-circuit current (J_{sc}) and the open-circuit voltages (V_{oc}). The numerical data are also summarized in Table 1. The $J_{sc}-N$ curve exhibits a volcano shape, whereas

Table 1. Cell Parameters of the H_2O_2-PFCs under Illumination of Simulated Sunlight (AM 1.5, 100 mW cm^{-2}, 1 sun)

photoanode	N	V_{oc} (V)	J_{sc} (mA cm^{-2})	J_{max} (mA cm^{-2})	P_{max} (mW cm^{-2})
ms-$BiVO_4$	1	0.59	0.068	0.034	0.0092
ms-$BiVO_4$	3	0.54	0.61	0.26	0.075
ms-$BiVO_4$	5	0.58	0.67	0.37	0.11
ms-$BiVO_4$	7	0.59	0.79	0.44	0.13
ms-$BiVO_4$	10	0.61	0.81	0.46	0.13
ms-$BiVO_4$	15	0.61	0.58	0.29	0.09
mp-TiO_2	[a]	0.31	0.01	0.007	0.0015

[a]The thickness of mp-TiO_2 film was ∼4 μm.

V_{oc} is almost independent of N at ≥ 1. The ms-$BiVO_4$/FTO (N = 10) photoanode cell provides J_{sc} = 0.81 mA cm^{-2} and V_{oc} = 0.61 V much greater than the values for the mp-TiO_2/FTO photoanode cell (J_{sc} = 0.01 mA cm^{-2} and V_{oc} = 0.31 V) under the same irradiation conditions. Clearly, there exists an optimal thickness of ms-$BiVO_4$. These experiments were carried out in deaerated electrolyte solution to prove that H_2O_2 works both as a fuel and an oxidant in this cell. However, the presence of O_2 was confirmed to hardly affect the cell performances (Figure S3).

The photocurrent was measured under irradiation of monochromatic light whose wavelength (λ_{ex}) continuously varied. The incident photon-to-current efficiency (IPCE) was calculated by the equation IPCE = $J_{ph}N_Ahc/IF\lambda$, where J_{ph} is the photocurrent, N_A is Avogadro constant, h is Planck constant, c is the speed of light, I is the light intensity, F is Faraday constant, and λ is the wavelength of the light. Figure 6A shows the IPCE action spectrum of the H_2O_2-PFC. The photocurrent rises at λ_{ex} = 500 nm, which is in agreement with the absorption edge of the ms-$BiVO_4$/FTO electrode. Also, the IPCE action spectrum well traces the absorption spectrum of the ms-$BiVO_4$/FTO electrode in Figure 2B (Figure S4). Further, the IPCE value at λ_{ex} = 400 nm reaches 6% at λ_{ex} = 400 nm, which is as much as 60 times greater than the value of the prototype of H_2O_2-PFC using the mp-TiO_2/FTO photoanode.[14] Finally, the effect of light intensity (I) on the cell performance was studied for the one-compartment H_2O_2-PFC. Figure 6B shows the maximum power density (P_{max}) as a function of I. The P_{max} increases with an increase in I to reach a saturated value of 0.13 mW cm^{-2} at I > 1 sun (100 mW cm^{-2}).

DOI: 10.1021/acsomega.8b01333
ACS Omega 2018, 3, 12099−12105

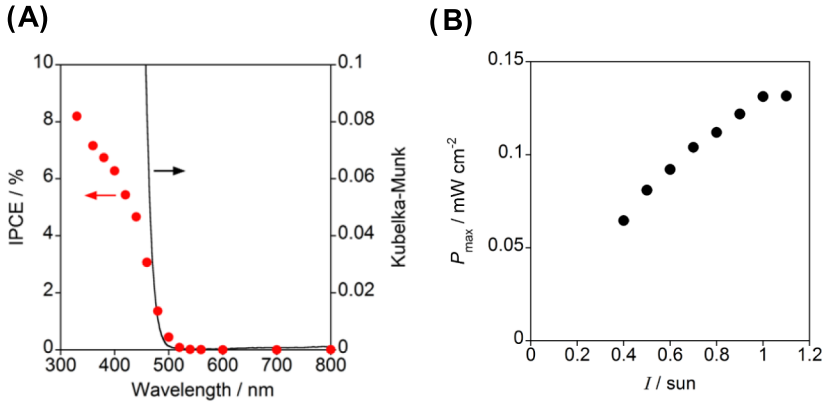

Figure 6. (A) IPCE action spectrum for the two-electrode cell with the structure of $BiVO_4$/FTO photoanode (N = 10)|deaerated electrolyte solution of 0.1 M $NaClO_4$ with 0.1 M H_2O_2 (pH 3)|PB/FTO cathode under the illumination of simulated solar light (AM 1.5, 100 mW cm^{-2}, 1 sun). (B) Maximum power density (P_{max}) as a function of light intensity (I) for the H_2O_2-PFC.

The present H_2O_2-PFC using ms-$BiVO_4$/FTO photoanode is considered to operate via the mechanism explained as follows (Scheme 2). Under irradiation of simulated sunlight,

Scheme 2. Action Mechanism Proposed for the Solar-Driven H_2O_2-PFC Using ms-$BiVO_4$/FTO as the Photoanode[a]

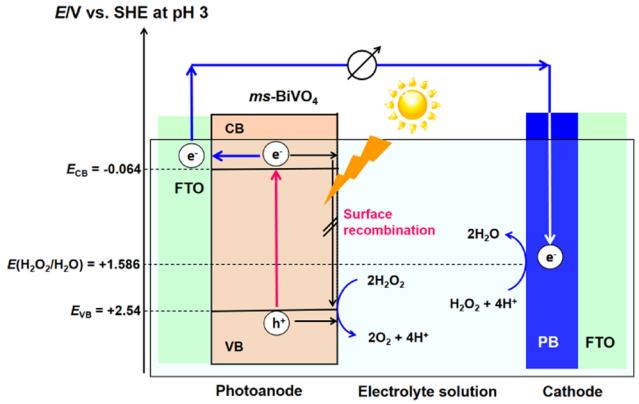

[a]The E_{CB} of ms-$BiVO_4$ was cited from ref 31, and the E_{VB} was estimated using the E_{CB} value and the E_g of 2.60 eV.

the ms-$BiVO_4$/FTO photoanode absorbs light at λ < 500 nm and the electrons in the VB are excited to the CB. The VB-holes (E_{VB} = +2.44 V vs SHE at pH 3) can oxidize H_2O_2 to produce O_2 with $E(O_2/H_2O_2)$ = +0.518 V vs SHE at pH 3 (eq 1).[32] Importantly, the surface recombination of the unmodified $BiVO_4$ photoanode can be effectively suppressed in the oxidation of H_2O_2, whereas it undergoes significant surface recombination in the H_2O oxidation.[33] Simultaneously, the CB-electrons (E_{CB} = −0.064 V at pH 3 vs SHE) are transported to the FTO electrode, and further to the PB/FTO cathode through the external circuit, taking part in the reduction of H_2O_2 to H_2O with $E(H_2O_2/H_2O)$ = +1.586 V (vs SHE at pH 3)[32] (eq 2). According to this scheme, the theoretical $V_{oc,theo}$ can be determined to be 1.65 V from eq 3.[34] As the film thickness of ms-$BiVO_4$ increases, the light absorption is enhanced, whereas the probability of the electrons to reach the the electron-collecting FTO electrode decreases due to the recombination in the bulk. Consequently, the balance between them would determine an optimum thickness of the ms-$BiVO_4$ film.

$$V_{oc,theo} = E(H_2O_2/H_2O) - E_{CB}(BiVO_4) \quad (3)$$

The practical power-generating efficiency of FCs (ε_{FC}) is expressed by eq 4.[14]

$$\varepsilon_{FC} = \varepsilon_{theo} \times \varepsilon_v \times \varepsilon_c \quad (4)$$

where ε_{theo} is the theoretical power-generating efficiency and ε_v and ε_c are the voltage efficiency and the current efficiency, respectively.

Because the ε_{theo} is 119%[14] and the voltage efficiency (ε_v) is given by 0.571 (=0.61/1.068 V) for the H_2O_2-PFC with N = 10, the maximum ε_{FC} can be estimated to be 68% by assuming the current efficiency to be 100% in this H_2O_2-PFC. However, the V_{oc} of the present cell (~0.6 V) is much smaller than the $V_{oc,theo}$ value (1.65 V) for which the overpotential for H_2O_2 reduction at the cathode is partly responsible. Also, van de Krol and co-workers have shown that the IPCE of the PEC cell for water splitting with $BiVO_4$/FTO as the photoanode can be drastically boosted by doping W^{6+} ions into $BiVO_4$ and intervening a SnO_2 layer between $BiVO_4$ and FTO.[35] Thus, there is still plenty of room for improvement in the present H_2O_2-PFC performances by exploring cathode materials and enhancing the electron transport in the ms-$BiVO_4$ film and charge collection at the interface with the back-contact.

CONCLUSIONS

This study has shown that monoclinic scheelite (ms)-$BiVO_4$ possesses the basic properties required for the photoanode of H_2O_2-PFC. A solar-driven one-compartment H_2O_2-PFC using ms-$BiVO_4$ as the photoanode and Prussian blue as the cathode provides J_{sc} = 0.81 mW cm^{-2} and V_{oc} = 0.61 V under illumination of simulated solar light (AM 1.5, 1 sun), and the incident photon-to-current efficiency at the excitation wavelength of 400 nm exceeds 6%. We anticipate that the performance can be further improved by reducing the losses during the electron transport in the photoanode and at the interface between the back-contact.

EXPERIMENTAL SECTION

Synthesis of ms-$BiVO_4$ Particles. The $BiVO_4$ particles were synthesized by the method reported in the literature.[36] $Bi(NO_3)_3 \cdot 5H_2O$, 0.2 M, and 0.2 M NH_4VO_3 were completely dissolved in dilute nitric acid (500 mL, volume ratio: concn HNO_3/H_2O = 1:4) by gentle stirring at room temperature for 1 h. After the addition of 1.66 M urea to the solution, the

DOI: 10.1021/acsomega.8b01333
ACS Omega 2018, 3, 12099−12105

mixed solution was heated at 80 °C for 8 h. Precursor particles thus prepared were harvested from the solution by centrifugal separation and then repetitively washed with purified water and vacuum dried at room temperature. The samples were then heated at 400 °C under an air atmosphere for 1 h to form the $BiVO_4$ particles.

Preparation and Characterization of Electrodes. $BiVO_4$/FTO electrodes were prepared by the metal−organic decomposition method.[37] Mixed solution of acetic acid (15 mL) containing 0.6 mol/L $Bi(NO_3)_3{\cdot}5H_2O$ and acetylacetone (75 mL) containing 0.04 M $VO(acac)_2$ was spin-coated on fluorine-doped tin oxide (FTO) film-coated glass substrate (20 × 20 mm^2, <10 Ω/sq) at a rotation speed of 500 rpm for 30 s at room temperature. After this process was repeatedly conducted for N cycles, the as-obtained films were heated in air at 673 K for 4h to form $BiVO_4$/FTO. The film thickness of $BiVO_4$/FTO was determined by cross-sectional SEM observation of the photoanode with Hitachi S-4800 Type II. The PB films were electrochemically deposited on FTO (PB/FTO) from an aqueous mixed solution of 0.02 M $FeCl_3{\cdot}6H_2O$ and 0.02 M $K_3[Fe(CN)_6]$ according to the method described in the literature.[38] Electrodeposition of the PB films on FTO was conducted by flowing a constant current of −40 $\mu A\ cm^{-2}$ for 10 min. The film thickness (l_{PB}) was estimated to be 0.94 μm. The X-ray diffraction (XRD) analysis was carried out with a Rigaku SmartLab X-ray diffractometer. Diffuse reflectance UV−vis spectra of the photoanodes were recorded on a UV-2600 spectrometer (Shimadzu) with integrating sphere unit (Shimadzu, ISR-2600Plus) at room temperature. The reflectance (R_∞) of the photoanodes was measured with respect to a standard sample ($BaSO_4$), and the Kubelka−Munk function ($F(R_\infty)$) defined by the equation of $F(R_\infty) = (1 - R_\infty)^2/2R_\infty$ was plotted against the wavelength. The Raman spectroscopy was carried out with a JASCO NRS-1000 laser Raman spectrometer at room temperature. Green laser with an emission wavelength of 532 nm was used as an excitation source.

Photocatalytic Decomposition of H_2O_2. Deaerated aqueous solutions of 0.1 M H_2O_2 solutions (10 mL, pH 3) containing $BiVO_4$ powder (10 mg, specific surface area = 0.673 $m^2\ g^{-1}$) were irradiated by simulated sunlight without (AM 1.5, 19 mW cm^{-2}) and with an optical cutoff filter (λ > 430 nm, AM 1.5, 15 mW cm^{-2}) at 25 °C. The amount of O_2 was determined by gas chromatography (Shimadzu, GC-8A).[14] For comparison, the same experiments were carried out using anatase TiO_2 particles (10 mg, specific surface area = 309 $m^2\ g^{-1}$, ST-01, Ishihara Sangyo).

Evaluation of Photofuel Cell Performances. The photoelectrochemical (PEC) response of the photoanodes incorporated in three-electrode PEC cells was evaluated by the measurements of current (J)−electrode potential (E) curves and decay curves of photocurrent at the rest potential under the irradiation of simulated solar light (AM 1.5, 100 mW cm^{-2}, 1 sun). Current (J)−cell voltage (V_{cell}) curves and power density−J curves were measured to determine the cell performance of two-electrode H_2O_2 PFCs. The action spectra of the incident photon-to-current conversion efficiency (IPCE) were measured by the same method as recently reported.[14]

■ ASSOCIATED CONTENT

Supporting Information

The Supporting Information is available free of charge on the ACS Publications website at DOI: 10.1021/acsomega.8b01333.

Tauc plots for ms-$BiVO_4$/FTO (Figure S1); time courses for O_2 generation from water in the ms-$BiVO_4$ particles under illumination of simulated sunlight (Figure S2); influence of O_2 on the cell performances (Figure S3); IPCE action spectrum (Figure S4) (PDF)

■ AUTHOR INFORMATION

Corresponding Author

*E-mail: h-tada@apch.kindai.ac.jp.

ORCID

Hiroaki Tada: 0000-0001-8638-0697

Notes

The authors declare no competing financial interest.

■ ACKNOWLEDGMENTS

This work was partially supported by a Grant-in-Aid for Scientific Research (C) No. 15K05654, and MEXT-Supported Program for the Strategic Research Foundation at Private Universities.

■ REFERENCES

(1) Teranishi, M.; Naya, S.; Tada, H. Temperature- and pH-Dependences of Hydrogen Peroxide Formation from Molecular Oxygen by Gold Nanoparticle-Loaded Titanium (IV) Oxide Photocatalyst. *J. Phys. Chem. C* **2016**, *120*, 1083−1088.

(2) Reidl, H.-J.; Pfleiderer, G. Production of Hydrogen Peroxide. U.S. Patent US2215883A1940.

(3) Teranishi, M.; Naya, S.; Tada, H. In Situ Liquid-Phase Synthesis of Hydrogen Peroxide from Molecular Oxygen Using Gold Nanoparticle-Loaded Titanium (IV) Dioxide Photocatalyst. *J. Am. Chem. Soc.* **2010**, *132*, 7850−7851.

(4) Tsukamoto, D.; Shiro, A.; Shiraishi, Y.; Sugano, Y.; Ichikawa, S.; Tanaka, S.; Hirai, T. Photocatalytic H_2O_2 Production from Ethanol/O_2 System Using TiO_2 Loaded with Au−Ag Bimetallic Alloy Nanoparticles. *ACS Catal.* **2012**, *2*, 599−603.

(5) Moon, G.-H.; Kim, W.; Bokare, A. D.; Sung, N.-E.; Choi, W. Solar Production of H_2O_2 on Reduced Graphene Oxide−TiO_2 Hybrid Photocatalysts Consisting of Earth-Abundant Elements Only. *Energy Environ. Sci.* **2014**, *7*, 4023−4028.

(6) Shiraishi, Y.; Kanazawa, S.; Sugano; Tsukamoto, D.; Sakamoto, H.; Ichikawa, S.; Hirai, T. Highly Selective Production of Hydrogen Peroxide on Graphitic Carbon Nitride ($g\text{-}C_3N_4$) Photocatalyst Activated by Visible Light. *ACS Catal.* **2014**, *4*, 774−780.

(7) Kaynan, N.; Berke, B. A.; Hazut, O.; Yerushalmi, R. Sustainable Photocatalytic Production of Hydrogen Peroxide from Water and Molecular Oxygen. *J. Mater. Chem. A* **2014**, *2*, 13822−13826.

(8) Fuku, K.; Sayama, K. Efficient Oxidative Hydrogen Peroxide Production and Accumulation in Photoelectrochemical Water Splitting Using a Tungsten Trioxide/Bismuth Vanadate Photoanode. *Chem. Commun.* **2016**, *52*, 5406−5409.

(9) Drew, K.; Girishkumar, G.; Vinodgopal, K.; Kamat, P. V. Boosting Fuel Cell Performance with a Semiconductor Photocatalyst: TiO_2/Pt−Ru Hybrid Catalyst for Methanol Oxidation. *J. Phys. Chem. B* **2005**, *109*, 11851−11857.

(10) Kaneko, M.; Nemoto, J.; Ueno, H.; Gokan, N.; Ohnuki, K.; Horikawa, M.; Saito, R.; Shibata, T. Photoelectrochemical Reaction of Biomass and Bio-related Compounds with Nanoporous TiO_2 Film Photoanode and O_2-Reducing Cathode. *Electrochem. Commun.* **2006**, *8*, 336−340.

DOI: 10.1021/acsomega.8b01333
ACS Omega 2018, 3, 12099−12105

(11) Horiuchi, Y.; Toyao, T.; Takeuchi, M.; Matsuoka, M.; Anpo, M. Recent Advances in Visible-Light-Responsive Photocatalysts for Hydrogen Production and Solar Energy Conversion—from Semiconducting TiO_2 to MOF/PCP Photocatalysts. *Phys. Chem. Chem. Phys.* **2013**, *15*, 13243−13253.
(12) Lianos, P. Review of Recent Trends in Photoelectrocatalytic Conversion of Solar Energy to Electricity and Hydrogen. *Appl. Catal., B* **2017**, *210*, 235−254.
(13) Mase, K.; Yoneda, M.; Yamada, Y.; Fukuzumi, S. Seawater Usable for Production and Consumption of Hydrogen Peroxide as a Solar Fuel. *Nat. Commun.* **2016**, *7*, No. 11470.
(14) Fujiwara, K.; Akita, A.; Kawano, S.; Fujishima, M.; Tada, H. Hydrogen Peroxide-Photofuel Cell using TiO_2 Photoanode. *Electrochem. Commun.* **2017**, *84*, 71−74.
(15) Fujishima, A.; Zhang, X.; Tryk, D. A. TiO_2 Photocatalysis and Related Surface Phenomena. *Surf. Sci. Rep.* **2008**, *63*, 515−582.
(16) Iyatani, K.; Horiuchi, Y.; Moriyasu, M.; Fukumoto, S.; Cho, S.-H.; Takeuchi, M.; Matsuoka, M.; Anpo, M. Development of Separate-Type Pt-Free Photofuel Cells on Visible-Light Responsive TiO_2 Photoanode. *J. Mater. Chem.* **2012**, *22*, 10460−10463.
(17) Iyatani, K.; Horiuchi, Y.; Fukumoto, S.; Takeuchi, M.; Anpo, M.; Matsuoka, M. Separate-Type Pt-Free Photofuel Cell Based on a Visible-Responsive TiO_2 Photoanode: Effect of Hydrofluoric Acid Treatment of the Photoanode. *Appl. Catal., A* **2013**, *458*, 162−168.
(18) Park, Y.; McDonald, K. J.; Choi, K.-S. Progress in Bismuth Vanadate Photoanodes for Use in Solar Water Oxidation. *Chem. Soc. Rev.* **2013**, *42*, 2321−2337.
(19) Wood, P.; Glasser, F. P. Preparation and Properties of Pigmentary Grade $BiVO_4$ Precipitated from Aqueous Solution. *Ceram. Int.* **2004**, *30*, 875−882.
(20) Shaegh, S. A. M.; Nguyen, N.-T.; Ehteshami, S. M. M.; Chan, S. H. A Membraneless Hydrogen Peroxide Fuel Cell Using Prussian Blue as Cathode Material. *Energy Environ. Sci.* **2012**, *5*, 8225−8228.
(21) Akita, A.; Masuda, T.; Fujiwara, K.; Fujishima, M.; Tada, H. One-Compartment Hydrogen Peroxide-Photofuel Cell Using TiO_2 Photoanode and Prussian Blue Cathode. *J. Electrochem. Soc.* **2018**, *165*, F300−F304.
(22) Kudo, A.; Omori, K.; Kato, H. A Novel Aqueous Process for Preparation of Crystal Form-Controlled and Highly Crystalline $BiVO_4$ Powder from Layered Vanadates at Room Temperature and its Photocatalytic and Photophysical Properties. *J. Am. Chem. Soc.* **1999**, *121*, 11459−11467.
(23) Tokunaga, S.; Kato, H.; Kudo, A. Selective Preparation of Monoclinic and Tetragonal $BiVO_4$ with Scheelite Structure and Their Photocatalytic Properties. *Chem. Mater.* **2001**, *13*, 4624−4628.
(24) Zhang, A.; Zhang, J. Hydrothermal processing for obtaining of $BiVO_4$ nanoparticles. *Mater. Lett.* **2009**, *63*, 1939−1942.
(25) Yu, J.; Kudo, A. Effects of Structural Variation on the Photocatalytic Performance of Hydrothermally Synthesized $BiVO_4$. *Adv. Funct. Mater.* **2006**, *16*, 2163−2169.
(26) Galembeck, A.; Alves, O. L. $BiVO_4$ Thin Film Preparation by Metalorganic Decomposition. *Thin Solid Films* **2000**, *365*, 90−93.
(27) Zhao, Z.; Li, Z.; Zou, Z. Electronic Structure and Optical Properties of Monoclinic Clinobisvanite $BiVO_4$. *Phys. Chem. Chem. Phys.* **2011**, *13*, 4746−4753.
(28) Serpone, N.; Lawless, D.; Khairutdinov, R. Size Effects on the Photophysical Properties [Kudo, A of Colloidal Anatase TiO_2 Particles: Size Effects on the Photophysical Properties of Colloidal Anatase TiO_2 Particles: Size Quantization versus Direct Transitions in This Indirect Semiconductor? *J. Phys. Chem.* **1995**, *99*, 16646−16654.
(29) Kudo, A.; Miseki, Y. Heterogeneous Photocatalyst Materials for Water Splitting. *Chem. Soc. Rev.* **2009**, *38*, 253−278.
(30) Laursen, A. B.; Man, I. C.; Trinhammer, O. L.; Rossmeisl, J.; Dahl, S. The Sabatier Principle Illustrated by Catalytic H_2O_2 Decomposition on Metal Surfaces. *J. Chem. Educ.* **2011**, *88*, 1711−1715.
(31) Long, M.; Cai, W.; Kisch, H. Visible Light Induced Photoelectrochemical Properties of n-$BiVO_4$ and n-$BiVO_4$/p-Co_3O_4. *J. Phys. Chem. C* **2008**, *112*, 548−554.
(32) Electrochemical Society of Japan. *Denki Kagaku Binran (Handbook of Electochemistry)*; Maruzen Publishing: Tokyo, 2000.
(33) Zhong, D. K.; Choi, S.; Gamelin, D. R. Near-Complete Suppression of Surface Recombination in Solar Photoelectrolysis by "Co−Pi" Catalyst-Modified W:$BiVO_4$. *J. Am. Chem. Soc.* **2011**, *133*, 18370−18377.
(34) Masuda, T.; Fujishima, M.; Tada, H. Photo-Effect on the Electromotive Force in Two-Compartment Hydrogen Peroxide-Photofuel Cell. *Electrochem. Commun.* **2018**, *93*, 31−34.
(35) Liang, Y.; Tsubota, T.; Mooij, L. P. A.; van de Krol, R. Highly Improved Quantum Efficiencies for Thin Film $BiVO_4$ Photoanodes. *J. Phys. Chem. C* **2011**, *115*, 17594−17598.
(36) Kotani, S.; Kudo, A.; Nakagaki, R.; Tokumura, K. Novel Synthesis Method of Visible-Light-Responsive Bismuth Vanadate Fine Powder, a Photocatalyst Consisting of the Fine Powder, and a Purification Method Using the Fine Powder Photocatalyst. Japanese Published Unexamined Application No. 2004-24936.
(37) Sayama, K.; Nomura, A.; Arai, T.; Sugita, T.; Abe, R.; Yanagida, S.; Oi, T.; Iwasaki, Y.; Abe, Y.; Sugihara, H. Photoelectrochemical Decomposition of Water into H_2 and O_2 on Porous $BiVO_4$ Thin-Film Electrodes under Visible Light and Significant Effect of Ag Ion Treatment. *J. Phys. Chem. B.* **2006**, *110*, 11352−11360.
(38) Itaya, K.; Akahoshi, H.; Toshima, S. Electrochemistry of Prussian Blue-Modified Electrodes: An Electrochemical Preparation Method. *J. Electrochem. Soc.* **1982**, *129*, 1498−1500.

DOI: 10.1021/acsomega.8b01333
ACS Omega 2018, 3, 12099−12105